

ARTICLE

Open Access

A nanogenerator based on metal nanoparticles and magnetic ionic gradients

Jingyu Wang^{1,2}, Tao Xiao^{1,2}, Jiahui Guo^{1,2}, Xing Zhao¹ and Yong Yan^{1,2,3}

Abstract

Developing a new technique/method and/or mechanism for separating ionic charges is critical to the fabrication of a high-performance nanogenerator. Inspired by charge migration and/or separation under an electric bias, herein, we demonstrate a reverse process in which the ionic charge gradients within a metal nanoparticle film are used to output electrical energy. The metal nanoparticle core is ‘jammed’ within the film, while the counterion itself is mobile and magnetic; therefore, ionic gradients are created through an external magnetic field. The distribution gradient of magnetic counterions is subsequently transformed into an electric potential within the metal nanoparticle film and into an electron flow in the external circuit. The performance of the nanoparticle nanogenerator is also optimized, and the highest output open-circuit voltage reaches 0.55 V. Finally, we develop a continuum charge-transport model combining Poisson and Nernst–Planck diffusion equations to simulate the production of electrical energy within metal nanoparticle films.

Introduction

Generating micro/nano electrical energy by converting other types of energy (e.g., mechanical, heat, chemical, etc.) has become increasingly important for widely distributed wearable electronic devices^{1–3}. In these micro- and/or nanogenerators, mechanical energy, for example, induces the separation of positive and negative charges within the ‘active’ materials, which gives rise to a potential difference between the electrodes and ultimately leads to the output of electricity^{4–6}. Specifically, the underlying mechanisms for electricity generation involves the effective separation of ionic charges, which determines the performance of a nanogenerator. Ionic charge separation can be achieved by the piezoelectric effect^{7,8}, the triboelectric effect^{9,10}, electrochemical polarization^{5,11}, gradients of temperature^{12,13}, and humidity^{14,15}; however, developing a new technique/method and/or proposing a new mechanism is always challenging.

On the other hand, metals have not played the same role as semiconductors in modern electronics because their electrical properties are largely independent of the potential that is applied to them^{16–19}. We have previously shown that this limitation in bulk metals can be overcome at the nanoscale when metal nanoparticles are functionalized with charged organic ligands^{20–23}. An electric field induces the movement of mobile counterions and generates ionic gradients within metal nanoparticle films, enabling the fabrication of diodes, sensors, transistors, and logic circuits^{20,21,23}. The separation of ionic charges is a key step in a nanogenerator: can we use this counterion gradient within a metal nanoparticle film to produce electrical energy? Instead of the electric field, other types of energy (technique/method) should be considered to create the counterion gradient within a nanoparticle film.

In this study, we propose a magnetic force that induces the migration of magnetic counterions. The magnetic counterion is a paramagnetic DyCl_4^- anion whose magnetic susceptibility is high enough to ensure its movement within metal nanoparticle films. Under an external magnetic field, the gradient distribution of magnetic counterions sets up a

Correspondence: Yong Yan (yany@nanoctr.cn)

¹CAS Key Laboratory of Nanosystem and Hierarchical Fabrication, CAS Center for Excellence in Nanoscience, National Center for Nanoscience and Technology, Beijing 100190, China

²University of Chinese Academy of Sciences, Beijing 100049, China

Full list of author information is available at the end of the article

© The Author(s) 2023



Open Access This article is licensed under a Creative Commons Attribution 4.0 International License, which permits use, sharing, adaptation, distribution and reproduction in any medium or format, as long as you give appropriate credit to the original author(s) and the source, provide a link to the Creative Commons license, and indicate if changes were made. The images or other third party material in this article are included in the article's Creative Commons license, unless indicated otherwise in a credit line to the material. If material is not included in the article's Creative Commons license and your intended use is not permitted by statutory regulation or exceeds the permitted use, you will need to obtain permission directly from the copyright holder. To view a copy of this license, visit <http://creativecommons.org/licenses/by/4.0/>.

potential difference within a metal nanoparticle film and then outputs electrical energy.

Results

To fabricate a metal nanoparticle nanogenerator, magnetic organic ligands are first synthesized²⁴. Positively charged N,N,N-trimethyl(11-mercaptoundecyl)ammonium chloride (HS-C11NMe₃⁺Cl⁻, TMA) molecules are mixed with DyCl₃ to prepare magnetic TMA ligands with negatively charged paramagnetic counterions DyCl₄⁻. Compared with TMA molecules, the UV-vis spectrum of mag-TMA shows several weak peaks at approximately 755 nm, 804 nm, and 907 nm, which could be ascribed to the absorption of dysprosium ions²⁵ (Fig. S1). In addition, electrospray ionization mass spectrometry (ESI-MS) measurements confirmed the synthesis of DyCl₄⁻ anions (Fig. S2). The mag-TMA ligands are subsequently used to functionalize gold nanoparticles²⁰ (AuNPs, 5.6 ± 0.8 nm in diameter, see TEM in Fig. 1a). Magnetization curve measurements, M-H (magnetization-magnetic field intensity), performed at room temperature indicate that the TMA AuNPs are diamagnetic ($\chi_g \sim -4.0 \times 10^{-5}$ emu/g), while the mag-TMA

AuNPs are paramagnetic ($\chi_g \sim 7.4 \times 10^{-5}$ emu/g), which is consistent with the value reported for other magnetic anions²⁶ (Fig. 1b).

The nanogenerator is then fabricated by drop-casting an ~1- μ m-thick thin film of mag-TMA AuNPs from a methanolic solution on a silica substrate with e-beam deposited Au/Cr (65/5 nm) electrodes (Fig. 1c and Fig. S3). When a magnetic field acts on device, the magnetic mobile counterions DyCl₄⁻ tend to migrate toward and accumulate around the electrode close to the magnet (Fig. S4). This is confirmed by energy-dispersive spectroscopy (EDS) measurements (see Fig. 1d for EDS mapping and Fig. 1e for distribution profiles). Since the nanoparticle core is ‘jammed’ within the film, Au does not change across the channel. In contrast, the concentrations of both Cl and Dy increase on the magnet side, showing a distribution gradient for DyCl₄⁻ counterions within the nanoparticle film.

The distribution gradient of magnetic counterions is subsequently transformed into an electric potential within the metal nanoparticle film. To minimize the electrostatic energy created by this potential difference, electrons are

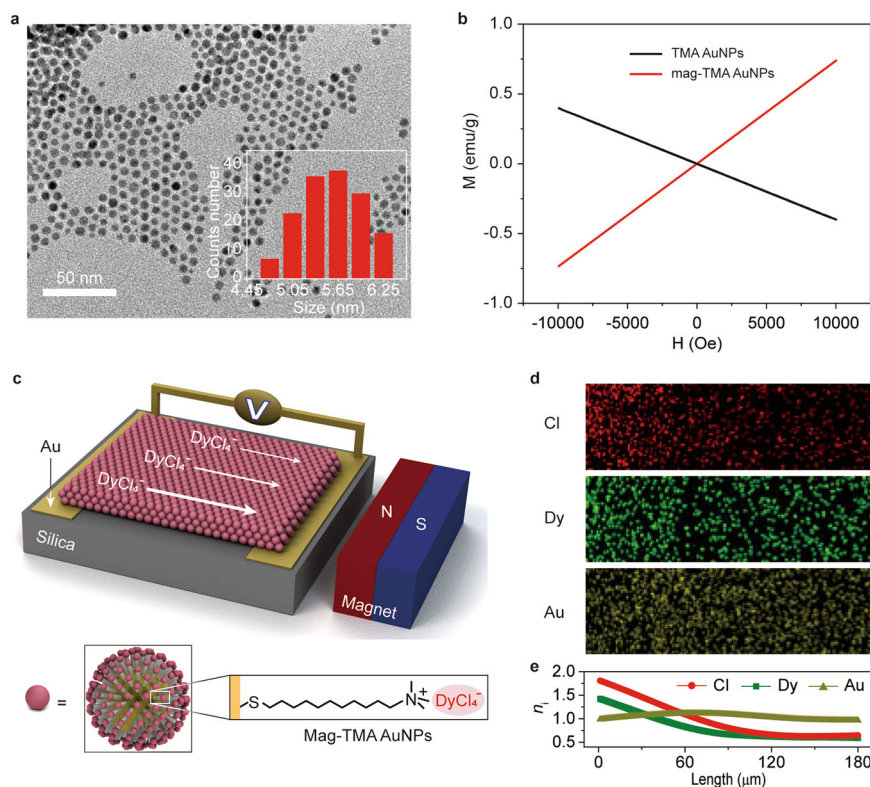


Fig. 1 Scheme of the device and demonstration of magnetic ionic gradients. **a** TEM image of AuNPs and particle size statistics. **b** M-H curves of TMA and mag-TMA AuNPs. **c** The top scheme illustrates the metal nanoparticle nanogenerator in which the magnetic counterions (DyCl₄⁻) migrate toward the electrode close to the magnet. The bottom scheme shows an individual mag-TMA gold nanoparticle and one of its magnetic ligands with an associated DyCl₄⁻ counterion. **d** EDS mapping of Cl, Dy, and Au elements within the mag-TMA AuNP film after placing a magnet (200 mT) on the left side of the film for approximately 10 min. **e** Corresponding profiles of Cl, Dy, and Au elemental distributions.

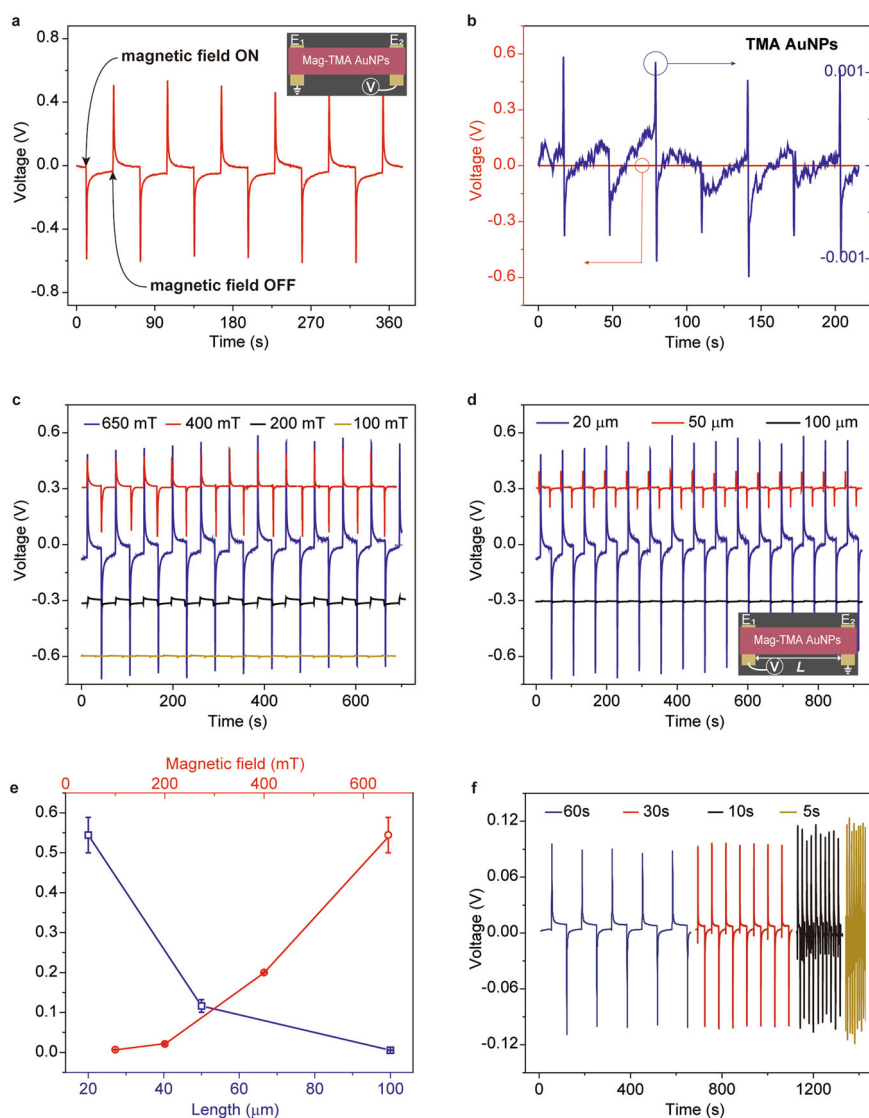


Fig. 2 The electrical output of the mag-TMA AuNP nanogenerator. **a** Open-circuit voltage of the mag-TMA AuNP nanogenerator when the magnetic field is applied (ON) and removed (OFF). **b** The output characteristics of a control device fabricated by using TMA AuNPs in which the counterions (Cl^-) are nonmagnetic. The red curve (left y-axis) is magnified and replotted in the blue curve (right y-axis). **c, d** Dependence of open-circuit voltages on the strength of the magnetic field (**c**) and channel length L between two electrodes (**d**). For the sake of clarity, the red/black/yellow curves are manually shifted upward/downward by 0.3 V/0.6 V. All of the channel lengths in (**c**) are 20 μm , and the magnetic fields in (**d**) are 650 mT. **e** The open-circuit voltage amplitudes as a function of channel length (blue curve, bottom x-axis) and magnetic field strength (red curve, top x-axis). **f** The dependence of open-circuit voltages on the frequencies of the ON/OFF magnetic field. All of the channel lengths are 50 μm , and the magnetic fields are 650 mT.

injected into the nanoparticle film from the electrode that is farther away from the magnet. Consequently, electron flow is detected in the external circuit, leading to the output of electrical energy. This corresponds to the ‘ON’ state when the magnetic field is placed (see the first peaks in the output voltages/currents in Fig. 2 and Fig. S5). When the magnetic field is removed, the negatively charged magnetic counterions that previously accumulated are prone to diffuse back to their original positions. In this case, electron will be injected from the other

electrode that was close to the magnet. This is the process for outputting a voltage/current in the opposite direction (see the first and second peaks in Fig. 2a, Fig. S5a, b). Reversible switching between the ‘ON’ and ‘OFF’ phases of the magnetic field produces alternating outputs that are very similar to those of previous nanogenerators (e.g., piezoelectric, triboelectric).

The reliability of electricity generation by the mag-TMA AuNP nanogenerator is confirmed by reversing the lead connections. Both the open-circuit voltages and short-circuit

currents have reversed polarity (Fig. S5a vs. b). In another experiment, when the magnetic DyCl_4^- counterions are replaced by nonmagnetic Cl^- anions, no apparent open-circuit voltage is measured in TMA AuNP films (Fig. 2b). The trace potential (~ 0.001 V) observed during the switching of the magnetic field is probably due to electromagnetic induction from the closed loops. This control experiment not only indicates the negligible impacts of electromagnetic induction but also confirms that the output of the mag-TMA AuNP nanogenerator originates from the magnetic field-induced distribution gradient of magnetic counterions. In addition, charge separation that is induced by a magnetic field is a new finding in nanogenerators and is apparently different from previous nanogenerators. The transport characteristics of the mag-TMA AuNP nanogenerator are shown in Fig. S6, indicating that the contact between the electrodes and nanoparticles is Ohmic.

Next, factors that impact the output performance of the mag-TMA AuNP nanogenerator are studied. The first is the strength of the magnetic field. For a given channel length (20 μm), an increase in the magnetic field intensity generally increases the magnitude of the electrical output (Fig. 2c). With a 650 mT magnetic field, an open-circuit voltage of ~ 0.55 V is recorded. However, as the field decreases to 100 mT, no apparent voltage is measured. We also find that the output performance is dependent on the channel length of the device. Figure 2d shows the open-circuit voltage of the nanoparticle nanogenerator recorded with several channel lengths ranging from 20 to 100 μm under a constant magnetic field (650 mT). Under the same circumstances, the smaller the lengths of device channels are, the larger the voltage generated. We attribute this to the likelihood that the number of ions reaching the electrode decreases significantly with increasing channel distance. This is an important finding since it suggests a roadmap for future performance gains that can accompany device miniaturization (Fig. 2e). In addition, the influence of the switching frequency of the magnetic field on the device performance is also studied. Figure 2f shows the output signal of the device under various switching frequencies ranging from 5 s to 60 s. A slight increase in output voltage is found at high frequency, which is probably due to the backflow of counterions that do not reach the equilibrium state, leading to an accumulation of effective counterions. The cycling performance of the device is also shown in Fig. S7.

To simulate electricity generation by mag-TMA AuNP films, a continuum charge-transport model combining Poisson and Nernst-Planck (PNP) diffusion equations is developed. In this model, only the mobile magnetic counterions and not the charged NPs can migrate in response to the local magnetic field and concentration gradients. Moreover, within the nanoparticle film, the motions of ions and electrons are related to each other to

maintain local charge neutrality. In addition, the conduction electrons can flow freely in and out of the nanoparticle film at the electrodes, whereas the counterions can only move within the nanoparticle film. For simplicity, we convert the magnetic force into an electric force. According to Maxwell's equations, the magnetic field generated by the magnetic counterions and their movements is much smaller than the external magnetic field, so it can be ignored.

Here, we considered a one-dimensional domain $[0, L]$. Since the magnetic counterions are negatively charged, the applied magnetic field can be converted into an electric field by using the transformation of force, $F_H = \chi_m HV \text{grad}H = qE$ (see the meaning of parameters in SI). For the transport of charged species i , the governing PNP equations could be simplified to $\frac{\partial c_i}{\partial t} = -\nabla \cdot J_i = -\nabla \cdot \left[-D_i (\nabla c_i + \frac{F}{RT} c_i z_i \nabla \phi) \right]$ and $\nabla \cdot (\nabla \epsilon_0 \epsilon \nabla \phi) = F \sum_i z_i c_i$ (see SI for details). With appropriate boundary conditions, the coupled PNP equations are then solved numerically by using a commercial finite element solver. The output voltage can be regarded as the charging and discharging of a capacitor. Therefore, the equation can be finally integrated

by $V_{\text{output}} = \begin{cases} V & V < V_{\text{max}} \\ V_{\text{max}} \exp(-tL/R_V \epsilon \epsilon_0) & V = V_{\text{max}} \end{cases}$ (see SI for details). The calculated concentration profiles (Fig. 3a) demonstrate that the counterions accumulate on the side close to the magnet and eventually reach equilibrium under a proper magnetic field, consequently influencing potential distribution (Fig. 3b) and ultimately transforming into an electric potential within the nanoparticle film (Fig. 3c) and an output voltage in the external circuit (Fig. 3d, e). In addition, with increasing magnetic field intensity, the output voltage also increases, which is consistent with the experimental results (Fig. 3d vs. 2c). This model also captures the increase in the output voltage due to a decrease in channel lengths between the electrodes (Fig. 3e, f).

Discussion

It is important to consider the shortcomings of our proof-of-concept devices. Before this nanogenerator can become a technologically viable alternative to any existing energy harvesting device, several aspects need to be considered. One is the strong magnetic field required for output electricity. A field of 650 mT is too strong to be practically useful. One solution might be to use counterions with much higher magnetic susceptibility²⁷ (e.g., $\text{Ln}(\text{hfa})_4^-$; $\text{Ln} = \text{Tb}, \text{Dy}, \text{Ho}, \text{Er}, \text{Tm}, \text{Yb}$; $\text{hfa} = 1,1,1,5,5,5$ -hexafluoro-acetylacetonate). The other could be designing magnetic core/shell nanoparticles^{28,29} (e.g., Ni/Au , $\text{Fe}_3\text{O}_4/\text{Au}$) in which the additional magnetic nanocores could enhance the gradient distribution of the magnetic field within the nanoparticle film. Second, the output performance—both the open-circuit voltage and especially the short-circuit current (\sim nano amperes)—is not

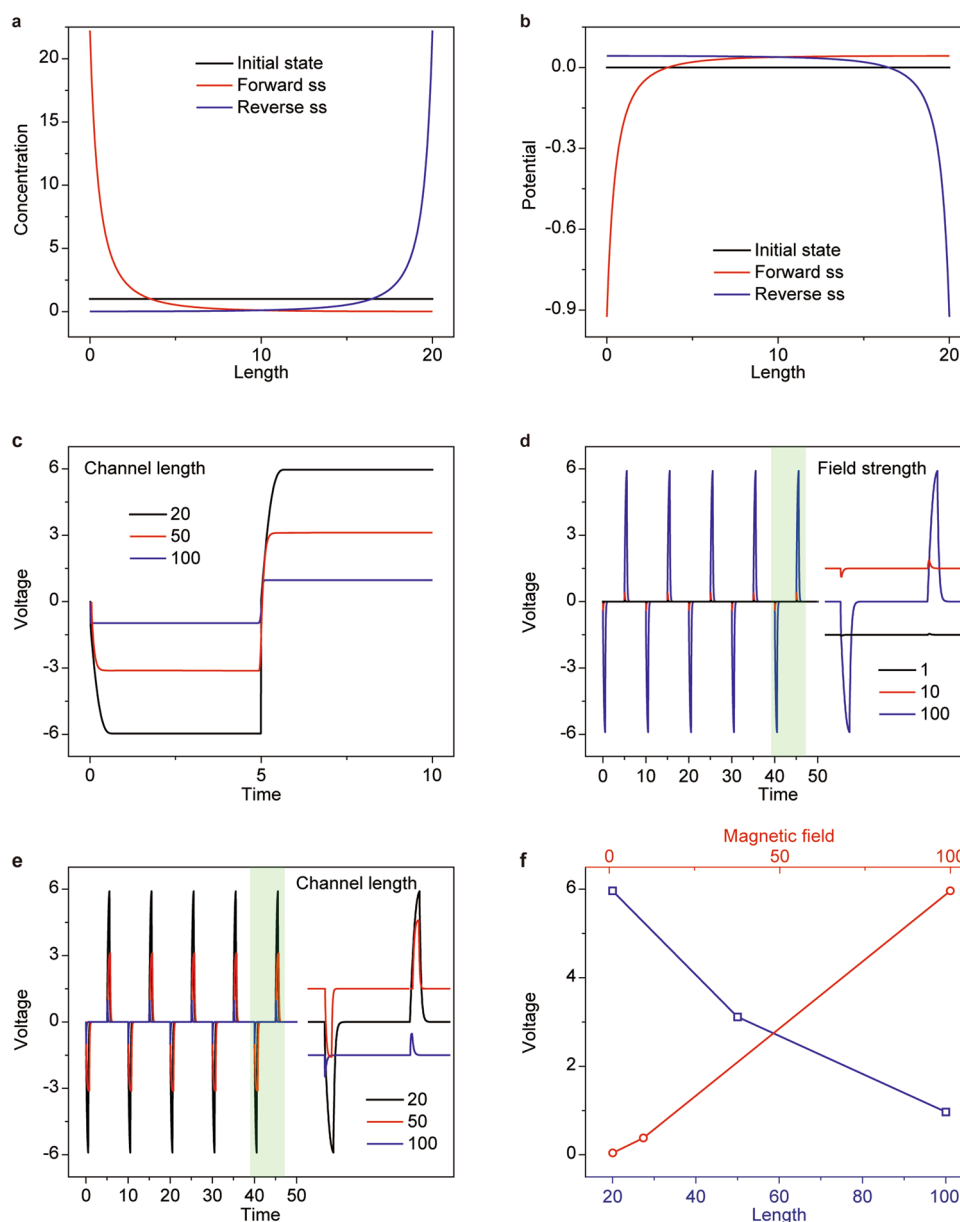


Fig. 3 Simulation of the mag-TMA AuNP nanogenerator. **a, b** Distributions of the DyCl_4^- counterions (**a**) and potentials (**b**) at the initial state, forward steady state, and reverse steady state. **c** Time-dependent voltage within the mag-TMA AuNP film. **d, e** Time-dependent open-circuit voltages as a function of the strength of the magnetic field (**d**) and channel length between two electrodes (**e**). The light-green highlighted regions are magnified and plotted on the right. For the sake of clarity, the red/black curves in (**d**) and red/blue curves in (**e**) are artificially moved upward/downward by 1.5. **f** The open-circuit voltage amplitudes as a function of channel length (blue curve, bottom x-axis) and magnetic field strength (red curve, top x-axis). Three magnetic fields (1, 10, and 100) and channel lengths (20, 50, and 100) are used for simulation. The magnetic field in (**a**) to (**c**) and (**e**) is 100, and the channel length in (**d**) is 20.

competitive with other nanogenerators. This is due to the low ‘effective’ counterion concentration and mobility ‘activated’ by the present magnetic field. Reducing channel length is demonstrated to be useful for improving the output performance (Fig. 2d, e). In addition, increasing the electrode surface area could be favorable for generating more current. We have tried to fabricate a sandwiched longitudinal device.

However, has proven to be challenging due to poor nanoparticle film quality, which leads to short-circuiting upon the deposition of the top electrode. Improving film quality by using other techniques is currently understudied. The last aspect can be the design of the nanogenerator. Manually switching the magnetic field ‘ON’ and ‘OFF’ is far from realistic in practical application. A possible solution is

rotating the device under the assistance of mechanical energy while keeping the magnetic field constantly applied.

Finally, we would like to emphasize the idea of separating charges by applying a magnetic field. The magnetic field induced the migration of magnetic counterions, which plays a role similar to that of an electric field. This new technique/method/mechanism is different from those of previous nanogenerators that are based on other phenomena, such as the piezoelectric effect, triboelectric effect, electrochemical polarization, gradients of temperature and humidity, and physical contact between two materials with different electron affinities. On the other hand, since charged metal nanoparticles can be used to fabricate various electronic components (e.g., sensors, diodes, and transistors), a magnetic nanoparticle nanogenerator can be integrated to power electronic components and circuits, enabling all-metal-nanoparticle systems.

Conclusions

In summary, we fabricated a nanogenerator based on charged metal nanoparticles with mobile magnetic counterions. The application of a magnetic field induces a distribution gradient of magnetic counterions, which subsequently transforms into an electric potential within the metal nanoparticle film and outputs electrical energy. The separation of ionic charges through the application of a magnetic field is a new finding that has not been demonstrated before. Although the performance of the metal nanoparticle generator is currently not competitive with other reports, we expect that in the future, with further improvements, this metal nanoparticle generator can be used in practical applications, especially in self-powered all-metal-nanoparticle electronics.

Materials and methods

AuNP synthesis

DDA AuNPs (5.5 ± 0.8 nm) were synthesized according to previous reports^{30,31}. Based on a typical procedure, $\text{HAuCl}_4 \cdot 3\text{H}_2\text{O}$ (0.12 mmol) was first dissolved in a toluene solution (13.2 mL) containing dodecylamine (DDA; 2.4 mmol) and dilauryldimethylammonium bromide (DDAB; 1.2 mmol). In a separate vial, tetrabutylammonium borohydride (TBAB; 0.2 mmol) and DDAB (0.6 mmol) were dissolved in toluene (5.7 mL). The TBAB solution was then injected into the gold salt solution under vigorous stirring for 12 h. This produced an ~ 3 nm Au nanoparticle seed. To prepare the growth solution, 1.2 mmol $\text{HAuCl}_4 \cdot 3\text{H}_2\text{O}$, 28.3 mmol DDA, and 4.5 mmol DDAB were dissolved in 113.4 mL toluene. The above seed solution was subsequently injected into the growth solution under vigorous stirring. A mixed solution of hydrazine monohydrate (5.8 mmol) and DDAB (4.5 mmol) in toluene (43.8 mL) was prepared and added dropwise into a HAuCl_4 solution over ~ 30 min under

vigorous stirring. After 12 h of reaction, 5.6 nm DDA AuNPs were produced.

Synthesis of mag-TMA ligands

To synthesize the mag-TMA ligands, 0.5 mmol *N,N,N*-trimethyl-(11-mercaptoundecyl)ammonium chloride (TMA) and 0.5 mmol DyCl_3 were first mixed in 1 mL methanol. After stirring for 24 h at room temperature, the mag-TMA ligands were obtained.

Surface functionalization of AuNPs with mag-TMA ligand

A DDA AuNP (30–50 mL) solution was first quenched by acetone. The NP precipitates were redispersed in toluene, and the mag-TMA (55 mg) CH_2Cl_2 solution (20 mL) was immediately added. The NP precipitates were washed with CH_2Cl_2 (20 mL) three times. Subsequently, 28 mg mag-TMA in 10 mL methanol was added to the NP precipitate. The ligand exchange reaction proceeded for 1 h, and the NPs were precipitated by the addition of toluene. After the mag-TMA AuNPs were washed with CH_2Cl_2 (3×20 mL), they were redispersed in 1.5 mL of methanol and filtered through a cellulose acetate 0.22 μm filter.

Characterization

ESI-MS analysis was conducted by using an LCMS/ESI/QTOF Analyzer (UPLC-QTOF). The UV-Vis absorption spectra were recorded by a spectrophotometer (Shimadzu, Japan, UV 2600). TEM was performed on a Tecnai G2 20 S-TWIN. EDS was performed on an SEM equipped with a Horiba EMAX X-ray detector (SEM, Hitachi-SU8220). The VSM measurement of AuNPs was performed on a PPMS-ANC300 (Quantum Design, America & attocube systems AG, Germany).

Device fabrication and electrical measurements

The gold electrodes (8 mm \times 1 mm \times 65/5 nm), Au/Cr were first deposited on a silica substrate by e-beam evaporation through a shadow mask. The mag-TMA AuNPs in methanol were subsequently drop-casted to cover the entire electrode. The electrical characteristics were measured by a Keithley 6517 high-precision electrometer, and the data were collected by an acquisition card. The magnetic field was provided by a 650 mT neodymium magnet. The time interval between the application and removal of the magnetic field was 30 s.

Acknowledgements

This work was supported by the National Natural Science Foundation of China (21875053) and the Strategic Priority Research Program of the Chinese Academy of Sciences (XDB36000000). The authors thank B. Tu and B. Lu for their helpful discussions and support on modeling.

Author details

¹CAS Key Laboratory of Nanosystem and Hierarchical Fabrication, CAS Center for Excellence in Nanoscience, National Center for Nanoscience and

Technology, Beijing 100190, China. ²University of Chinese Academy of Sciences, Beijing 100049, China. ³School of Chemistry and Biological Engineering, University of Science and Technology Beijing, Beijing 100083, China

Author contributions

J.W. carried out the experiments and, with the help of T.X., J.G., and X.Z. performed the data analysis. J.W. modeled the experimental results. All authors wrote the manuscript. Y.Y. conceived and supervised the project.

Conflict of interest

The authors declare no competing interests.

Publisher's note

Springer Nature remains neutral with regard to jurisdictional claims in published maps and institutional affiliations.

Supplementary information The online version contains supplementary material available at <https://doi.org/10.1038/s41427-023-00468-x>.

Received: 30 July 2022 Revised: 21 January 2023 Accepted: 1 February 2023.

Published online: 10 March 2023

References

- Zeng, W. et al. Fiber-based wearable electronics: a review of materials, fabrication, devices, and applications. *Adv. Mater.* **26**, 5310–5336 (2014).
- Fan, F. R., Tang, W. & Wang, Z. L. Flexible nanogenerators for energy harvesting and self-powered electronics. *Adv. Mater.* **28**, 4283–4305 (2016).
- Song, Y. D., Wang, N., Hu, C. S., Wang, Z. L. & Yang, Y. Soft triboelectric nanogenerators for mechanical energy scavenging and self-powered sensors. *Nano Energy* **84**, 105919 (2021).
- Yan, Y., Timonen, J. V. I. & Grzybowski, B. A. A long-lasting concentration cell based on a magnetic electrolyte. *Nat. Nanotechnol.* **9**, 901–906 (2014).
- Krabbenborg, S. O. & Huskens, J. Electrochemically generated gradients. *Angew. Chem. Int. Ed.* **53**, 9152–9167 (2014).
- Sun, Q. Q. et al. Surface charge printing for programmed droplet transport. *Nat. Mater.* **18**, 936–941 (2019).
- Wang, Z. L. & Song, J. H. Piezoelectric nanogenerators based on zinc oxide nanowire arrays. *Science* **312**, 242–246 (2006).
- Jia, Y. L. & Zhang, K. Piezoelectric potential-enhanced output and nonlinear response range for self-powered sensor on curved surface. *Nano Energy* **96**, 107103 (2022).
- Fan, F. R., Tian, Z. Q. & Wang, Z. L. Flexible triboelectric generator! *Nano Energy* **1**, 328–334 (2012).
- He, W. C. et al. Boosting output performance of sliding mode triboelectric nanogenerator by charge space-accumulation effect. *Nat. Commun.* **11**, 4277 (2020).
- Inagi, S., Ishiguro, Y., Atobe, M. & Fuchigami, T. Bipolar patterning of conducting polymers by electrochemical doping and reaction. *Angew. Chem. Int. Ed.* **49**, 10136–10139 (2010).
- Cheng, H. L. & Ouyang, J. Y. Ultrahigh thermoelectric power generation from both ion diffusion by temperature fluctuation and hole accumulation by temperature gradient. *Adv. Energy Mater.* **10**, 2001633 (2020).
- Zhao, D. et al. Ionic thermoelectric supercapacitors. *Energy Environ. Sci.* **9**, 1450–1457 (2016).
- Sun, Z. Y. et al. Nanofiber fabric based ion-gradient-enhanced moist-electric generator with a sustained voltage output of 1.1 volts. *Mater. Horiz.* **8**, 2303–2309 (2021).
- Li, L. H. et al. Moisture-driven power generation for multifunctional flexible sensing systems. *Nano Lett.* **19**, 5544–5552 (2019).
- Moreira, H. et al. Electron cotunneling transport in gold nanocrystal arrays. *Phys. Rev. Lett.* **107**, 176803 (2011).
- Zabet-Khosousi, A. & Dhirani, A. A. Charge transport in nanoparticle assemblies. *Chem. Rev.* **108**, 4072–4124 (2008).
- Kim, Y. et al. Stretchable nanoparticle conductors with self-organized conductive pathways. *Nature* **500**, 59–64 (2013).
- Yang, Y. J. et al. Stretchable energy-harvesting tactile interactive interface with liquid-metal-nanoparticle-based electrodes. *Adv. Funct. Mater.* **30**, 1909652 (2020).
- Yan, Y., Warren, S. C., Fuller, P. & Grzybowski, B. A. Chemo-electronic circuits based on metal nanoparticles. *Nat. Nanotechnol.* **11**, 603–608 (2016).
- Zhao, X. et al. Switchable counterion gradients around charged metallic nanoparticles enable reception of radio waves. *Sci. Adv.* **4**, eaau3546 (2018).
- Guo, J. H. et al. Counterion gradients around charged metal nanoparticles enabling basic electronics without semiconductors. *J. Phys. Chem. Lett.* **12**, 6102–6110 (2021).
- Zhao, X. et al. Charged metal nanoparticles for chemo-electronic circuits. *Adv. Mater.* **31**, e1804864 (2019).
- Brown, P. et al. Magnetic control over liquid surface properties with responsive surfactants. *Angew. Chem. Int. Ed.* **51**, 2414–2416 (2012).
- Yuan, H. B., Zhang, J. H., Yu, R. J. & Su, Q. Synthesis of rare earth sulfides and their UV-vis absorption spectra. *J. Rare Earth.* **27**, 308–311 (2009).
- Joseph, A. et al. Paramagnetic ionic liquids for advanced applications: a review. *J. Mol. Liq.* **218**, 319–331 (2016).
- Wu, K. G. & Shen, X. H. Designing a new type of magnetic ionic liquid: a strategy to improve the magnetic susceptibility. *New J. Chem.* **43**, 15857–15860 (2019).
- Freitas, M. et al. Highly monodisperse Fe₃O₄@Au superparamagnetic nanoparticles as reproducible platform for genosensing genetically modified organisms. *ACS Sens.* **1**, 1044–1053 (2016).
- Chaudhuri, R. G. & Paria, S. Core/Shell nanoparticles: classes, properties, synthesis mechanisms, characterization, and applications. *Chem. Rev.* **112**, 2373–2433 (2012).
- Jana, N. R. & Peng, X. G. Single-phase and gram-scale routes toward nearly monodisperse Au and other noble metal nanocrystals. *J. Am. Chem. Soc.* **125**, 14280–14281 (2003).
- Kalsin, A. M. et al. Electrostatic self-assembly of binary nanoparticle crystals with a diamond-like lattice. *Science* **312**, 420–424 (2006).